Climatological Characteristics of Atmospheric Rivers and Their Inland Penetration over the Western United States

JONATHAN J. RUTZ AND W. JAMES STEENBURGH

Department of Atmospheric Sciences, University of Utah, Salt Lake City, Utah

F. MARTIN RALPH

Scripps Institute of Oceanography, La Jolla, California

(Manuscript received 25 May 2013, in final form 26 September 2013)

ABSTRACT

Narrow corridors of water vapor transport known as atmospheric rivers (ARs) contribute to extreme precipitation and flooding along the West Coast of the United States, but knowledge of their influence over the interior is limited. Here, the authors use Interim European Centre for Medium-Range Weather Forecasts (ECMWF) Re-Analysis (ERA-Interim) data, Climate Prediction Center (CPC) precipitation analyses, and Snowpack Telemetry (SNOTEL) observations to describe the characteristics of cool-season (November–April) ARs over the western United States. It is shown that AR frequency and duration exhibit a maximum along the Oregon–Washington coast, a strong transition zone upwind (west) of and over the Cascade–Sierra ranges, and a broad minimum that extends from the ''high'' Sierra south of Lake Tahoe eastward across the central Great Basin and into the deep interior. East of the Cascade–Sierra ranges, AR frequency and duration are largest over the interior northwest, while AR duration is large compared to AR frequency over the interior southwest. The fractions of cool-season precipitation and top-decile 24-h precipitation events attributable to ARs are largest over and west of the Cascade–Sierra ranges. Farther east, these fractions are largest over the northwest and southwest interior, with distinctly different large-scale patterns and AR orientations enabling AR penetration into each of these regions. In contrast, AR-related precipitation over the Great Basin east of the high Sierra is rare. These results indicate that water vapor depletion over major topographic barriers is a key contributor to AR decay, with ARs playing a more prominent role in the inland precipitation climatology where lower or less continuous topography facilitates the inland penetration of ARs.

1. Introduction

Atmospheric rivers (ARs) are narrow corridors of strong vertically integrated water vapor transport (IVT) that are responsible for nearly 90% of the extratropical poleward water vapor transport despite covering only 10% of the available longitude (Newell et al. 1992; Newell and Zhu 1994; Zhu and Newell 1998). ARs are often aligned along and ahead of cold fronts associated with extratropical cyclones, and achieve their high water vapor content through transport from the tropics and/or local moisture convergence (Ralph et al. 2004; Bao et al. 2006; Stohl et al. 2008). Thus, many ARs are related to warm conveyor belts—moist, ascending airstreams located within the warm sector of extratropical cyclones (Browning 1971; Carlson 1980; Eckhardt et al. 2004; Sodemann and Stohl 2013). Because of strong water vapor transport and low static stability, ARs can produce heavy precipitation, particularly when directed toward topographical barriers (e.g., Neiman et al. 2002; Ralph et al. 2004; Junker et al. 2008). This orographic precipitation acts to decrease the water vapor transport as an AR penetrates inland.

The hydrometeorological extremes associated with ARs are well documented, especially along the West Coast of North America. Ralph et al. (2006) showed that all seven major flood events on Northern California's Russian River between October 1997 and February 2006 were associated with landfalling ARs. An intense AR produced destructive

Corresponding author address: Jonathan J. Rutz, Department of Atmospheric Sciences, University of Utah, 135 S. 1460 E, Rm. 819 (WBB), Salt Lake City, UT 84112.
E-mail: jon.rutz@utah.edu

DOI: 10.1175/MWR-D-13-00168.1

flooding during November 2006 over parts of Oregon and Washington (Neiman et al. 2008a), and the same region experienced a prolonged period of heavy rainfall during March 2005 owing to interactions between an AR and a mesoscale frontal wave (Ralph et al. 2011). Warner et al. (2012) showed that most of the heavy precipitation events over the coastal northwestern United States during the past 60 years were associated with AR conditions. Neiman et al. (2011) showed that ARs were associated not only with heavy rain, but with extreme streamflow on four watersheds in Washington based on satellite observations of ARs and stream gauge data. Beyond the West Coast of North America, high-impact weather associated with ARs has been documented over eastern North America, Great Britain, and Chile (e.g., Moore et al. 2012; Lavers et al. 2011; Viale and Nuñez 2011).

Recent studies by Ralph et al. (2011, 2013a) document the importance of persistent AR conditions in generating the most extreme storm-total rainfall and flooding. Using unique, long-term (6 yr) hourly observations of AR conditions at a coastal observing site operated by the National Oceanic and Atmospheric Administration's (NOAA's) Hydrometeorology Testbed (HMT; hmt.noaa.gov; Ralph et al. 2013b), they found that AR conditions lasted an average of 20 h, but the most persistent events (roughly the top 10%) lasted an average of 40 h and produced 7 times the streamflow found in average events (Ralph et al. 2013a). Thus, forecasting extreme precipitation and flooding in the region requires accurate prediction of both the intensity and duration of AR conditions, especially over key topographic obstacles and flood-prone drainages.

Some ARs extend across the Cascade–Sierra ranges, or across the mountains of Southern California and the Baja Peninsula, and contribute to heavy precipitation and flooding over the interior western United States. In January 1997, an AR contributed to heavy rain along the snow-covered eastern slopes of the Sierra Nevada, leading to flooding that inundated ~64 000 acres and produced $540 million (U.S. dollars) in damage along the Truckee, Carson, and Walker Rivers (U.S. Dept. of the Interior 2012; Rigby 1998). During January 2010, an inland-penetrating AR produced heavy precipitation (including numerous 2-day accumulation records for January) and flooding across the southwestern United States, especially Arizona (Neiman et al. 2013). At upper elevations during this event, snowpack snow-water equivalent (SWE) increased as much as 234 mm, a consequence of snow accumulations and/or the absorption of rain by the snowpack. In November 2006, an AR contributed to heavy rainfall (widespread accumulations of +12 cm with a maximum of 30 cm) and rapid high-elevation snowmelt that led to numerous road washouts, destroyed bridges, and lowland flooding in and around Glacier National Park (Bernhardt 2006).

Several recent studies have estimated the contribution of ARs to total cool-season (November–April) precipitation over the western United States. Dettinger et al. (2011) used precipitation observations from National Weather Service Cooperative Observer (COOP) sites in the western United States to examine the fraction of cool-season precipitation associated with landfalling ARs (hereafter the AR fraction) during water years 1998–2008. During this period, 20%–50% of the precipitation at most COOP sites in California, Oregon, and Washington fell on the day of or day following AR observation along the U.S. West Coast, as identified using Special Sensor Microwave Imager (SSM/I) retrievals of integrated water vapor (IWV) [ARs defined following Ralph et al. (2004) as contiguous regions $\geq$2000 km long and $\leq$1000 km wide with IWV $\geq$ 20 mm]. Similarly, Guan et al. (2010) found that 30%–40% of the snowpack SWE accumulation in the Sierra Nevada during water years 2004–10 occurred on the day before, of, or following AR observation (as described above) along the California coast. Farther inland, Dettinger et al. (2011) found lower AR fractions, especially over the southwestern United States, although Rutz and Steenburgh (2012) show that the AR fraction over the southwestern United States is larger if ARs crossing the west coast of the Baja Peninsula are considered [Dettinger et al. (2011) did not consider ARs crossing along the Baja Peninsula]. However, none of these studies attempt to identify ARs over the interior western United States or account for their spatial extent when quantifying AR-related precipitation.

This paper uses gridded atmospheric analyses and daily precipitation datasets (gridded and gauge) to expand our knowledge of cool-season ARs over the western United States. In particular, we use new methods to identify ARs in reanalysis data and examine their climatological characteristics (frequency, duration, and influence on precipitation) from the coast into the western interior. These methods, which have the potential for broader applications in weather, hydrological, and climate research and forecasting, are described in section 2, with results related to the frequency, duration, and seasonal precipitation and extreme events presented in sections 3–5. Discussions, conclusions, and future work are summarized in sections 6 and 7.

2. Data and methods

a. Data sources

We identify ARs using the Interim European Centre for Medium-Range Weather Forecasts (ECMWF)

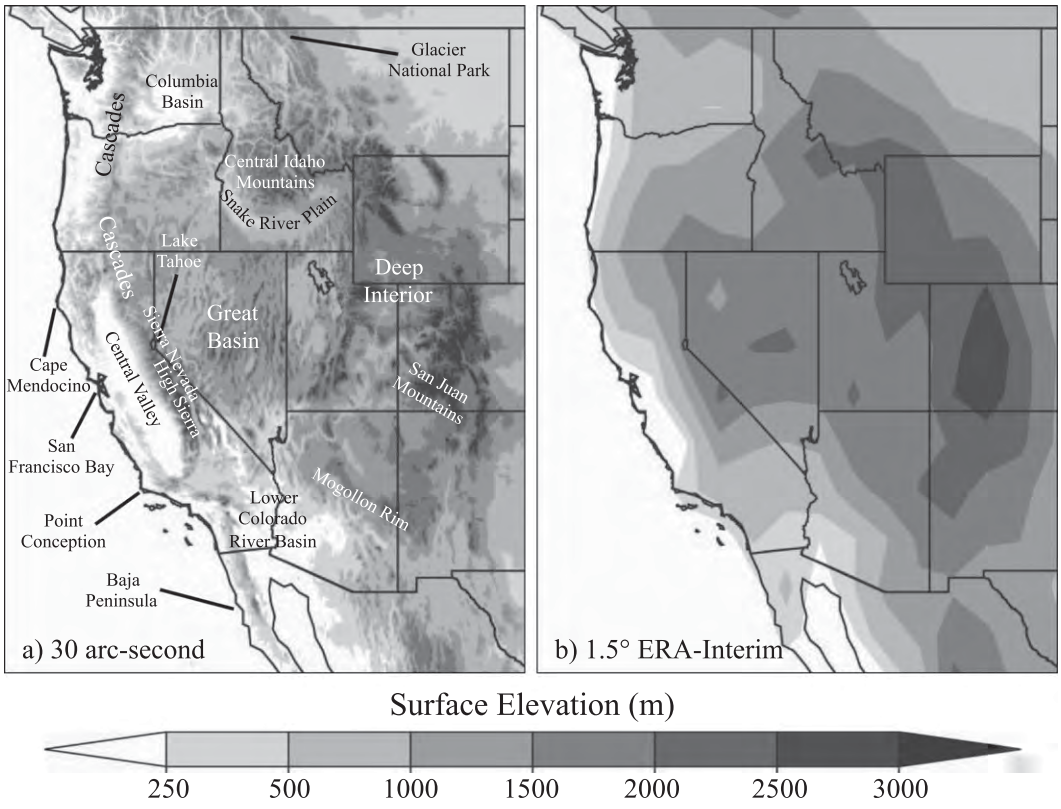

FIG. 1. (a) Observed (30 arc s) and (b) ERA-Interim (1.5°) topography (shaded in m) for the western United States. Geographic terms referenced in text are identified in (a).

Re-Analysis (ERA-Interim; Dee et al. 2011), which is based on a version of the ECMWF Integrated Forecast System (IFS) with 60 vertical levels (extending to 0.1 hPa), T255 triangular truncation for dynamical fields, and a reduced Gaussian grid with ~80-km spacing for surface and other gridpoint fields (Simmons et al. 2007; Uppala et al. 2008; Berrisford et al. 2009). The ~80-km Gaussian grid spacing provides a reasonable estimate of the effective grid spacing of the ERA-Interim in physical space (Kanamitsu 1989). The ERA-Interim data used here cover cool-season months (November–April) from November 1988 through April 2011, a total of 23 seasons, and was obtained from the ECMWF data server on a 1.5° latitude × 1.5° longitude grid with 6-h temporal resolution. Although the ERA-Interim provides sufficient spatial and temporal continuity for AR identification, neither the 1.5° grid nor the native ERA-Interim grid fully resolves the complex topography of the western United States (cf. Figs. 1a,b). This limited resolution may artificially smooth some subsynoptic-scale gradients, such as those associated with orographic processes over mountain barriers.

Precipitation observations and analyses come from the gridded NOAA/Climate Prediction Center (CPC) Unified Daily Precipitation Analysis (hereafter the CPC analysis) and the Snowpack Telemetry (SNOTEL) network of stations maintained by the National Resources Conservation Service (NRCS). The CPC analysis provides spatially continuous (0.25° grid spacing) 24-h precipitation analyses valid at 1200 UTC (Higgins et al. 2000). SNOTEL stations, using a large storage gauge and an Alter shield to reduce the effects of wind, provide automated precipitation observations at upper elevation sites (Hart et al. 2005; Rasmussen et al. 2011; USDA-NRCS 2012a,b).

SNOTEL observations are available both hourly and daily, but the latter are for 0000–0000 Pacific standard time (PST). To facilitate comparisons between SNOTEL observations and the CPC analysis, we use the hourly SNOTEL accumulated precipitation data to construct a set of 24-h accumulations valid at 1200 UTC. These data are quality controlled following Serreze et al. (1999) except that we allow the daily precipitation to be as large as 20 in. (~51 cm) instead of 10, and more than five standard deviations above the mean. This allows for the inclusion of some extreme events. Only sites that are operational throughout the study period are used.

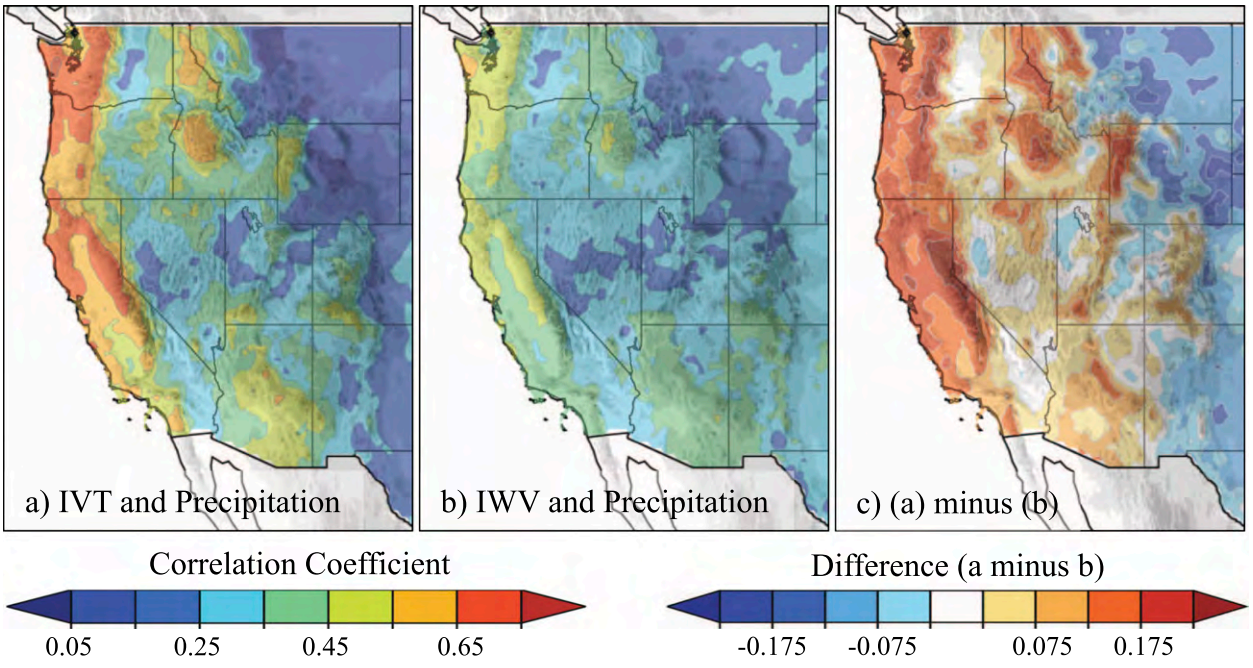

FIG. 2. (a) Correlation coefficient between the daily-mean (1200–1200 UTC) IVT and 24-h precipitation. (b) As in (a), but for daily mean IWV. (c) (a) minus (b).

b. Objective identification of atmospheric rivers

ARs are objectively identified in the ERA-Interim using two definitions. The first, IVT_{250}, defines an AR as a contiguous region ≥2000 km in length with IVT ≥ 250 kg m^{-1} s^{-1}. Here, IVT is defined as

$$\mathrm{IVT} = \frac{1}{g}\int_{p_{\mathrm{sfc}}}^{100\,\mathrm{hPa}} q\mathbf{V}\,dp, \qquad (1)$$

where g is the gravitational acceleration, q is the specific humidity, $\mathbf{V}$ is the total vector wind, p is pressure, and p_{sfc} is the surface pressure. The integration is done using data at the surface, 50-hPa intervals from the surface to 500 hPa, and 100-hPa intervals from 500 to 100 hPa. The second, IWV_{20}, defines an AR as a contiguous region ≥2000 km in length with IWV ≥ 20 mm. Here, IWV is defined as

$$\mathrm{IWV} = \frac{1}{g}\int_{p_{\mathrm{sfc}}}^{100\,\mathrm{hPa}} q\,dp, \qquad (2)$$

with the integration done as described above. Both IVT and IWV are then interpolated to the CPC analysis grid to facilitate the attribution of precipitation to ARs, as described in section 2c. In both cases, the AR length criterion is evaluated as the greatest distance between two points within each contiguous feature.

Previous work based on SSM/I satellite data uses IWV_{20} as a proxy for AR identification in lieu of the wind observations necessary to calculate IVT (e.g., Ralph et al. 2004; Neiman et al. 2008b; Dettinger et al. 2011). Whereas some results are presented based on IWV_{20}, we focus on IVT_{250} for two reasons. First, IVT is strongly related to precipitation over complex terrain (Junker et al. 2008; Neiman et al. 2002, 2013; Ralph et al. 2013a) and more strongly correlated with cool-season precipitation over most of the western United States than IWV (Fig. 2). Second, subjective evaluation of numerous AR events reveals that areas of IVT ≥ 250 kg m^{-1} s^{-1} crossing the West Coast of North America penetrate farther into the interior than coinciding areas of IWV ≥ 20 mm and correspond well with the spatial extent of heavy precipitation (e.g., Fig. 3). The use of IVT also aids in overcoming the limitations associated with the reduction of overall atmospheric thickness and IWV over elevated terrain.

In contrast to earlier studies (e.g., Ralph et al. 2004; Neiman et al. 2008b; Dettinger et al. 2011; Wick et al. 2013), AR width is not considered in the identification process. ARs identified using the IVT_{250} criteria rarely exceed 1000 km in width, whereas those that do still tend to possess AR characteristics (e.g., large length to width ratio and intense lower-tropospheric water vapor flux).

c. Attribution of precipitation to atmospheric rivers

The precipitation from the CPC analysis is defined as AR related if an AR is identified at a given grid point during any of the five 6-hourly analysis times during the 24-h accumulation period (1200–1200 UTC). For

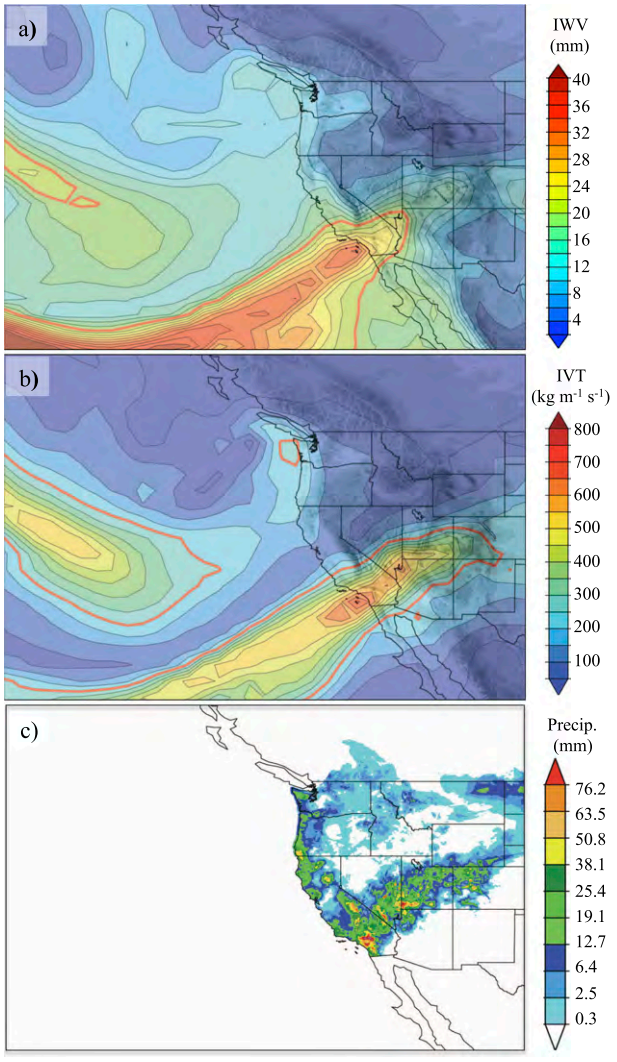

FIG. 3. ERA-Interim (a) IWV and (b) IVT at 0000 UTC 21 Dec 2010. Thick red lines in (a) and (b) denote threshold values of 20 mm and 250 kg m^{-1} s^{-1}, respectively. (c) Advanced Hydrological Prediction Services accumulated precipitation analysis for 24-h period ending 1200 UTC 21 Dec 2010.

precipitation at SNOTEL stations, the closest grid point is used to make this determination. We then define the AR fraction as the fraction of total cool-season precipitation that is AR related. To assess the role of ARs in major precipitation events, we also examine the fraction of top-decile 24-h precipitation events exceeding 0.1 in. (2.54 mm, the resolution of the SNOTEL data) that are AR related (hereafter top-decile fraction). By defining precipitation as AR-related only where ARs are observed, this approach is more geographically specific than earlier studies (e.g., Dettinger et al. 2011; Rutz and Steenburgh 2012), but the requirement of an AR to be present at only one analysis time is the most generous possible. Smaller AR fractions and top-decile fractions are obtained if an AR is required to be present at multiple analysis times.

3. AR frequency and duration

a. AR frequency

Based on IVT_{250}, the AR frequency (i.e., the fraction of 6-h analysis times meeting the AR identification criteria) over the western United States is characterized by a maximum (>15%) along the Oregon–Washington coast and a broad minimum (<5%) over the deep interior, southwest, and Great Basin east of the high Sierra (Fig. 4a, see Fig. 1 for geographic references). The coastal AR frequency decreases rapidly from Cape Mendocino south to Point Conception. East of the Cascade–Sierra ranges, the AR frequency is greatest over a low-elevation corridor that extends across the Columbia basin into northern Montana, and within the Snake River Plain and adjoining northern Great Basin.

For comparison, the IWV_{20} AR frequency is greatest along the coast of Northern California, with a decrease in frequency along the Oregon–Washington coast to the north and the central California coast to the south (Fig. 4b). Locations with an AR frequency >5% are limited to within ~100 km of the coast, with the greatest values found over the Columbia basin, Central Valley, and the lower Colorado River basin. Compared with IVT_{250}, fewer IWV_{20} ARs penetrate into the interior western United States except over the lower Colorado River basin (cf. Figs. 4a and 4b). Given that the IWV_{20} AR frequency over the interior is so low, as well as reasons discussed in the previous section, we focus on IVT_{250} ARs for the remainder of this paper.

The value of IVT chosen as a threshold to identify ARs affects the magnitude of AR frequency over the western United States, with lower (higher) thresholds yielding higher (lower) frequencies, but does not significantly alter the locations of AR frequency maxima or minima (cf. Figs. 4a and 5a,b). Changes in the observed pattern and magnitude of AR frequency found by varying the length criterion between 1500 and 2500 km are negligible (not shown).

The seasonality of AR frequency is characterized by a November maximum over the northern half of the western United States, but a more complex distribution over the southern half (Fig. 6). Much of Northern and central California, northwestern Nevada, eastern Arizona, and parts of western Colorado feature a December maximum, whereas a January maximum is found over Southern California, southern Nevada, extreme southwestern Utah, and western Arizona. Eastern Colorado features an

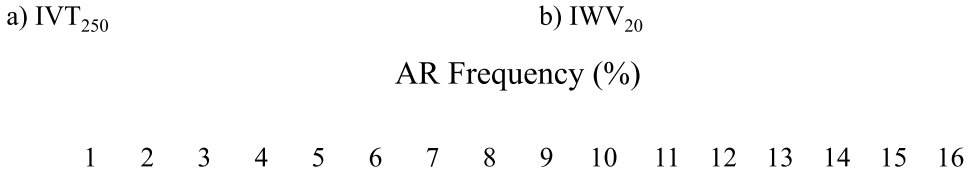

FIG. 4. Frequency of ERA-Interim analyses with AR conditions based on (a) IVT_{250} and (b) IWV_{20}.

April maximum, likely reflecting the contribution of low-level water vapor transport from the Gulf of Mexico during the spring. Histograms at selected coastal and interior locations further illustrate the AR seasonality. In the northern half of the western United States, coastal location A and interior location B observe a primary maximum in November and a secondary maximum in January, after which there is a monotonic decline in AR frequency during the latter half of the cool season. The monthly distribution at coastal locations C and E is quasi normal, and illustrates the increasingly later peak in AR frequency southward along the West Coast. Over the southern interior, events at locations D and F are relatively rare and the seasonality is not well defined.

b. AR duration

The mean AR duration, which is defined as the average number of hours of AR conditions experienced at a given location during an AR event (Ralph et al. 2013a), is greatest along the Oregon coast (23–24 h) and is collocated with the maximum in AR frequency (Fig. 7). Along the coast to the north and south of this maximum, the mean AR duration declines to ~19 h on the northwest tip of the Washington coast and ~17 h near Point Conception. East of the Cascade–Sierra ranges, the mean AR duration is greatest over the Columbia basin and northern Montana, within the Snake River Plain and adjoining northern Great Basin, and over Southern California, Arizona, and New Mexico. The mean AR duration is smallest (~12 h) along a corridor that extends from the high Sierra eastward across the central Great Basin and into the Rocky Mountains, aligning well with regions of smallest AR frequency. South of this corridor, the low AR frequency and higher AR duration suggests that ARs over the southwestern United States tend to be infrequent, but relatively long lived (cf. Figs. 4a and 7).

Because high-impact precipitation events are often the result of long-lived, persistent AR conditions (Ralph et al. 2011, 2013a; Moore et al. 2012), we also present histograms of AR duration at the same coastal and interior locations identified earlier. Both the coastal and interior locations have skewed distributions, but the latter have a greater frequency of short events and fewer long-duration events (Fig. 7). The frequency of AR events lasting only 6 h (i.e., one analysis time) nearly doubles from the coastal to the interior locations, whereas the frequency of AR events >12 h (i.e., three or more analysis times) decreases from ~50% at the coastal locations to ~20%–40% at the interior locations. Thus, there is a clear decline in duration of AR events from the coast

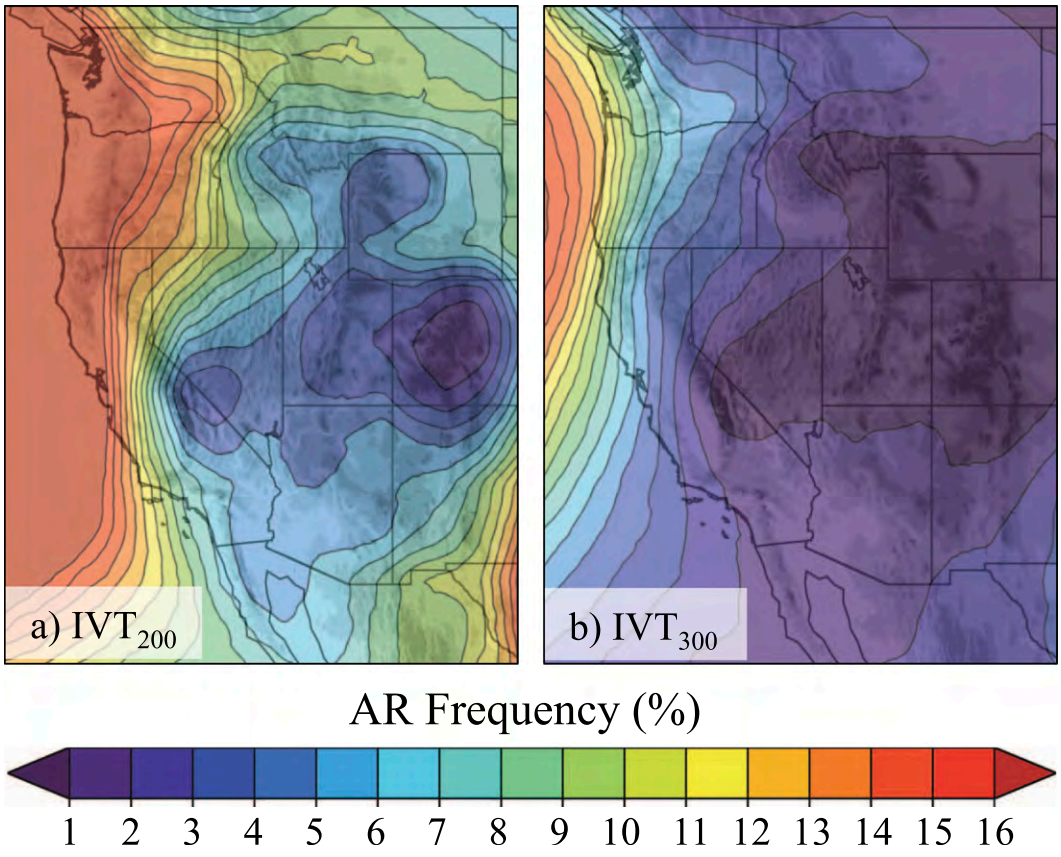

FIG. 5. Frequency of ERA-Interim analyses with AR conditions based on (a) IVT_{200} and (b) IVT_{300}.

to the interior. At location C, we find a mean AR duration of ~20 h, which agrees remarkably well with the independent and observationally based findings of Ralph et al. (2013a) at nearby Bodega Bay, California. Furthermore, our top-decile AR duration threshold of ~40 h (not shown) is also in very good agreement with their findings, although we note the difference in temporal resolution (6 h here, 1 h in Ralph et al. 2013a). These results increase confidence in the use of ERA-Interim analyses and the IVT_{250} definition used to identify ARs.

4. AR impacts on cool-season precipitation and extreme daily precipitation

a. Fraction of cool-season precipitation associated with AR events (''AR fraction'')

Based on the CPC analysis, the coastal AR fraction is largest (>0.60) north of San Francisco Bay, and decreases gradually to the south (Fig. 8a). A gradual decrease in AR fraction also extends from the West Coast to the lee of the Cascade–Sierra ranges, where a more abrupt decrease exists, particularly in the lee of the Sierra Nevada. A weaker gradient is found over Southern California where the topography is lower and less continuous than that of the high Sierra. The gradient in AR fraction found along the Cascade–Sierra ranges likely reflects water vapor depletion during orographic precipitation (e.g., Smith et al. 2005, 2010), resulting in fewer and/or less intense (i.e., smaller IVT) ARs farther inland.

Farther inland, the AR fraction is largest (~0.25–0.45) over the interior northwestern and southwestern United States, and smallest (<0.25) over the intermediate Great Basin. Over the interior northwestern United States, the strongest gradient occurs over the central Idaho mountains and northwestern Montana, whereas over the interior southwestern United States, the strongest gradient exists over the Mogollon Rim and higher terrain to the east and northeast. Low AR fraction values over the Great Basin extend eastward across Utah and join the broad minimum (<0.10) over the mountains and highlands of the deep interior.

There is generally good agreement between the AR fraction obtained using the CPC analysis and SNOTEL observations (cf. Figs. 8a,b), but some important differences exist. To highlight these differences, we select five geographic regions, each characterized by an AR frequency of ≥3% (see Fig. 4a), and compare the AR

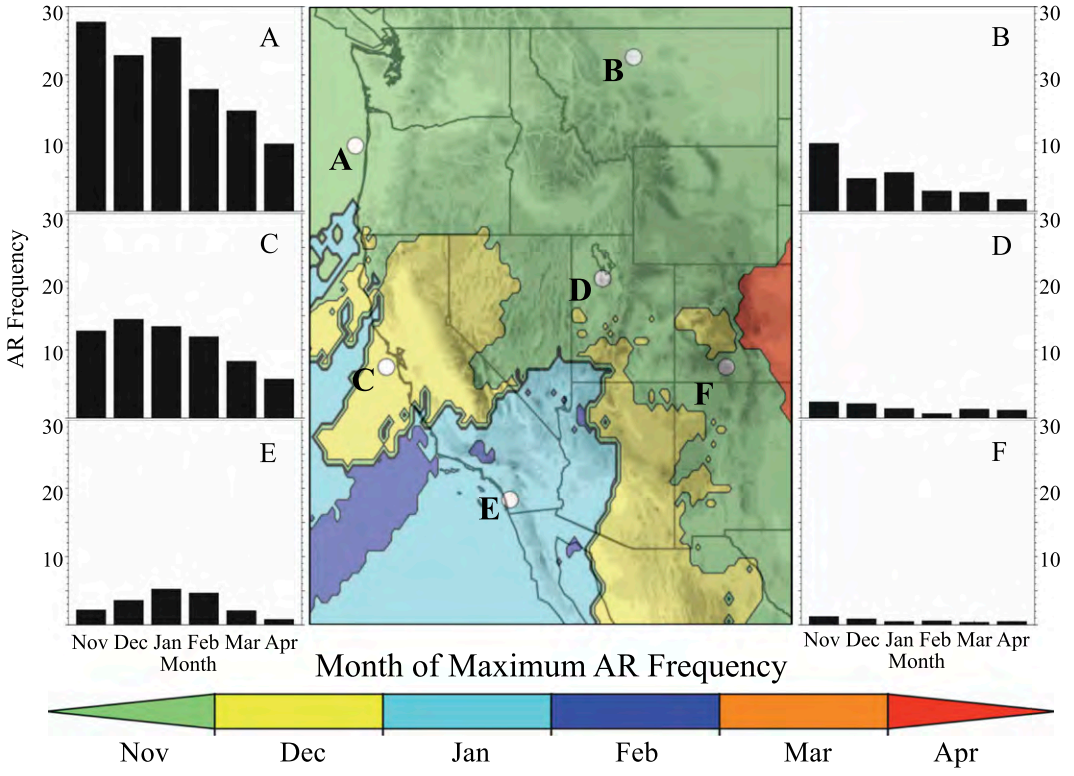

FIG. 6. Month of maximum AR frequency based on IVT_{250}. Histograms of IVT_{250} AR frequency by month at selected (left) coastal and (right) interior locations.

fraction obtained from the SNOTEL observations to that obtained by interpolating the CPC analysis to the SNOTEL locations. These five regions, identified in Fig. 8b, are the Cascades, the Sierra Nevada, the northern Rockies, northeast Oregon, and the southwest central Idaho mountains.

The AR fraction based on the interpolated CPC analysis is generally greater and less regionally varied than that based on the SNOTEL observations (Fig. 9). The median CPC AR fraction is 0.07 greater than the median SNOTEL AR fraction over the Sierra Nevada and 0.01–0.03 greater over the Cascades, northeast Oregon, and the southwest central Idaho mountains, all of which are significant at the 95% confidence level following Student's *t* test (used here and elsewhere for significance testing). Only over the northern Rockies is the median CPC AR fraction smaller (by 0.01) and this result is not significant at the 95% confidence level. The interquartile range in CPC AR fraction over the Cascades, Sierra Nevada, northeast Oregon, and the southwest central Idaho mountains is also smaller than those from the SNOTEL observations. For example, over the Cascades the interquartile range of the AR fraction based on the CPC analysis is only 0.04, but is 0.07 based on SNOTEL observations. Only over the northern Rockies is the interquartile range based on the CPC analysis greater. Thus, while the CPC AR fraction is characterized by a relatively smooth, monotonic decline from the coast to the interior, the AR fraction at SNOTEL stations indicates smaller-scale spatial variability embedded within this decline. This smaller-scale variability is likely due to the modulation of AR and non-AR precipitation by local and regional orographic effects.

The ratio of AR fraction to AR days [i.e., any 24-h accumulation period (1200–1200 UTC) period with AR-related precipitation] provides a measure of the dependence of total cool-season precipitation on the occurrence of a small number of ARs (Fig. 10). This ratio (multiplied by 100 for convenience) is largest (>3) over the southwestern United States, with a pronounced maximum over the high Sierra (>6), and smallest (<2) over the northwestern United States. This implies that a large fraction of the cool-season precipitation over the southwestern United States is produced by a small number of ARs, which is consistent with previous studies (Dettinger et al. 2011; Neiman et al. 2013). Secondary maxima exist over the San Juan Mountains, the southwest central Idaho mountains, portions of the adjoining Snake River Plain, and eastern Colorado, with the latter likely related to water vapor transport from the Gulf of Mexico.

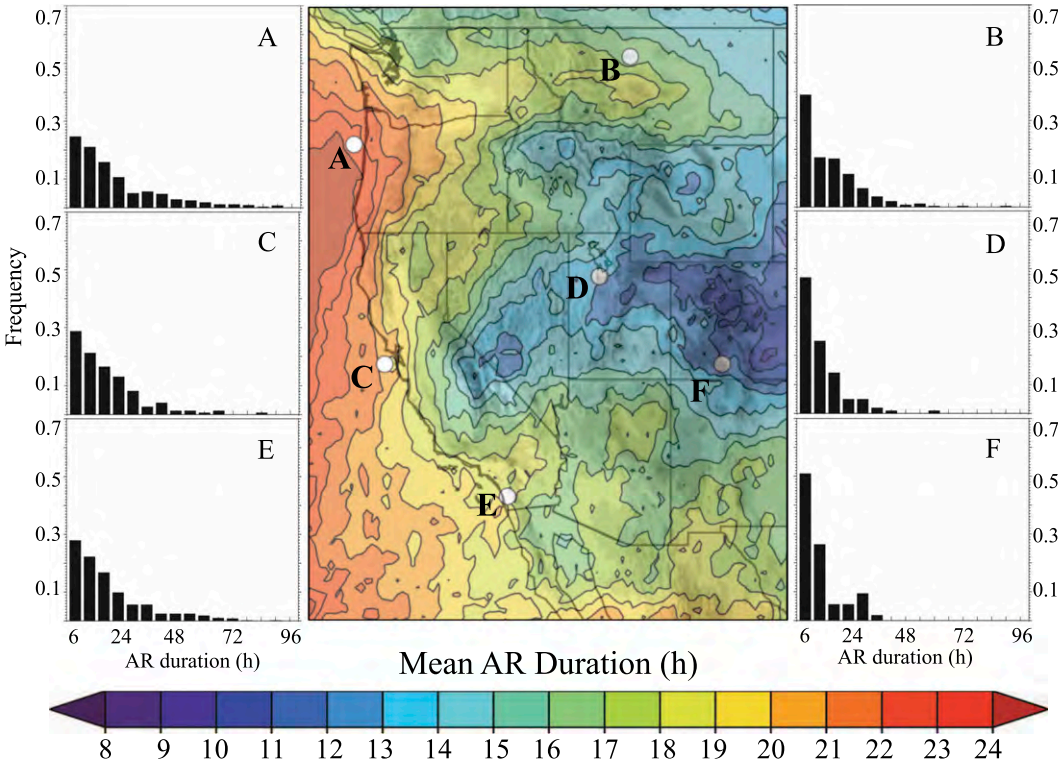

FIG. 7. Mean duration (h) of AR conditions based on IVT_{250}. Histograms of IVT_{250} AR duration at selected (left) coastal and (right) interior locations.

b. Fraction of top-decile 24-h precipitation events associated with ARs (''top-decile fraction'')

Based on the CPC analysis, the top-decile fraction follows a pattern similar to that of the AR fraction, but exhibits more spatial variability and stronger gradients (Fig. 11a, note that color-fill interval is double that for AR fraction). The top-decile fraction is largest (>0.75) along the coast north of San Francisco Bay and decreases along the coast to the south. Values decrease gradually inland from the coast before a more abrupt decrease in the lee of the Cascade–Sierra ranges. South of the Sierra Nevada, the top-decile fraction exhibits a well-defined gradient over the mountains of Southern California, which is less evident in the AR fraction.

East of the Cascade–Sierra ranges, the top-decile fraction is largest (>0.25) over portions of the interior northwestern and southwestern United States. Over the interior northwestern United States, the top-decile fraction is largest (>0.35) over the western part of the northern Rockies, northeast Oregon, and the southwest central Idaho mountains. These are mountain regions that are exposed to flow from the southwest and west. Transitions to lower fractions also exist as one moves eastward across the northern Rockies and northeastward across the central Idaho mountains. Over the southwestern interior, the top-decile fraction decreases over and northeast of the Mogollon Rim. The smallest top-decile fractions (<0.15) extend from the lee of the high Sierra eastward across the central Great Basin to the mountains and highlands of the deep interior.

There is generally good agreement between the spatial patterns of top-decile fraction using the CPC analysis and SNOTEL observations, but important differences are found at some locations (cf. Figs. 11a,b). To compare further, we examine the SNOTEL and interpolated CPC distributions within the five geographic regions identified earlier.

Similar to the results for the AR fraction, the top-decile fraction from the CPC analysis is generally greater and less regionally varied than that based on the SNOTEL observations (Fig. 12). The median CPC top-decile fraction is 0.14 greater than the median SNOTEL top-decile fraction over the Sierra Nevada, 0.03–0.04 greater over the Cascades, and the southwest central Idaho mountains, all of which are significant at the 95% confidence level. The median CPC top-decile fraction is 0.01–0.02 smaller over the northern Rockies and northeast Oregon, neither of which is significant at

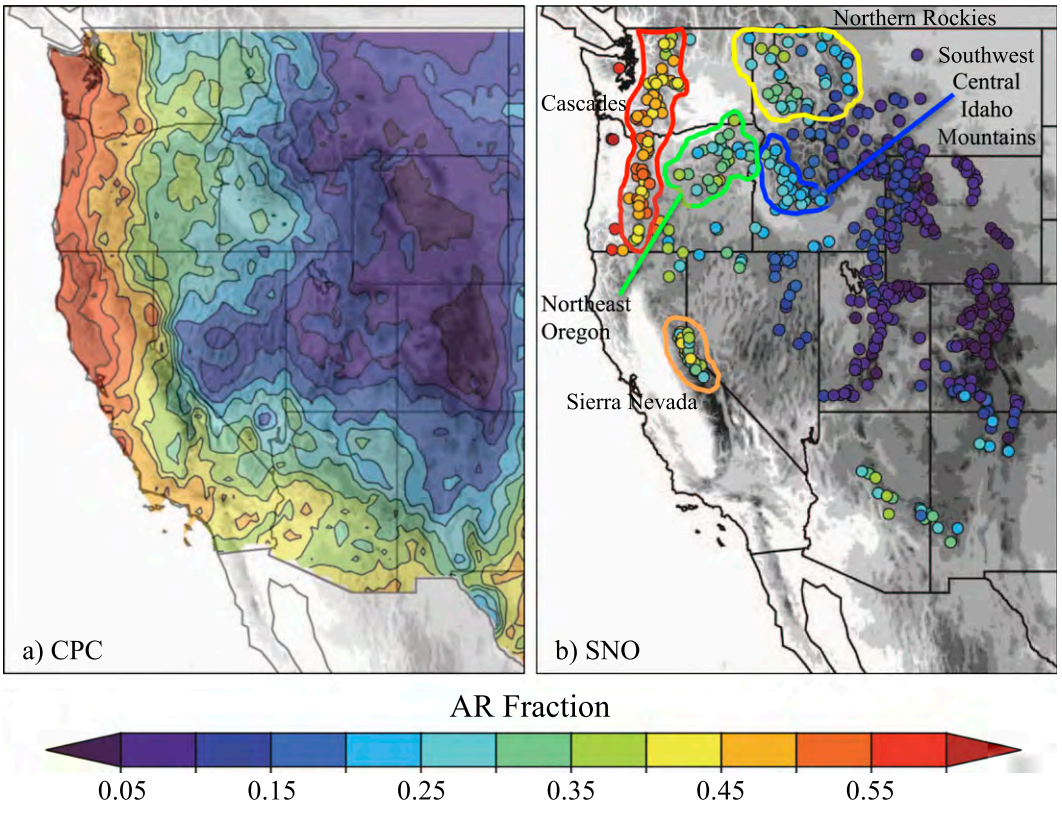

FIG. 8. IVT_{250} AR fraction (i.e., the fraction of cool-season precipitation associated with ARs) for (a) the CPC analysis and (b) SNOTEL stations. Selected regions referenced in text are highlighted in (b).

the 95% confidence level. The interquartile range of the CPC top-decile fraction over the Cascades, Sierra Nevada, and northeast Oregon is smaller than those from the SNOTEL observations, but is greater over the northern Rockies and the southwest central Idaho mountains. As for the AR fraction, these results suggest that the regional variability in top-decile precipitation is dependent on local and regional orographic effects. Furthermore, this variability, as measured by the interquartile range, is greater for the top-decile fraction than for AR fraction (cf. Figs. 9 and 12).

5. Penetration of ARs into the interior western United States: Pathways and synoptic patterns

To help illustrate preferred pathways for AR penetration into the interior without the need to track individual ARs, we compute the conditional frequency of AR conditions across the eastern Pacific and western United States in all analyses (i) 24 h prior to (−24 h) and (ii) during (0 h) the existence of AR conditions at five locations along the 111°W meridian. We use composite (i.e., mean) 500-hPa geopotential height analyses to illustrate the accompanying large-scale pattern. The resulting analysis illustrates the contrast in AR pathways and associated synoptic patterns over the northwest and southwest interior.

For the two locations over the northwest interior, the conditional frequency of AR conditions is largest in an elongated band that extends northeastward across the eastern Pacific Ocean and curves anticyclonically into the interior, with the largest values moving from near and upstream of the Oregon and Washington coast to the northwest interior from −24 to 0 h (Figs. 13a–d). The accompanying 500-hPa composite features a weakly progressive longwave pattern with enhanced southwesterly flow between a trough over the North Pacific and a ridge over the western United States. High conditional AR frequencies extend through the ridge axis at 0 h. In contrast, for the two locations over the southwest interior, the conditional frequency of AR conditions is largest off the California coast at −24 h. This maximum moves inland and exhibits weak cyclonic curvature at 0 h (Figs. 13g–j). The accompanying 500-hPa composite features a trough off the California coast that moves eastward over the southwest.

For the location over northern Utah, the conditional frequency of AR conditions at −24 h features

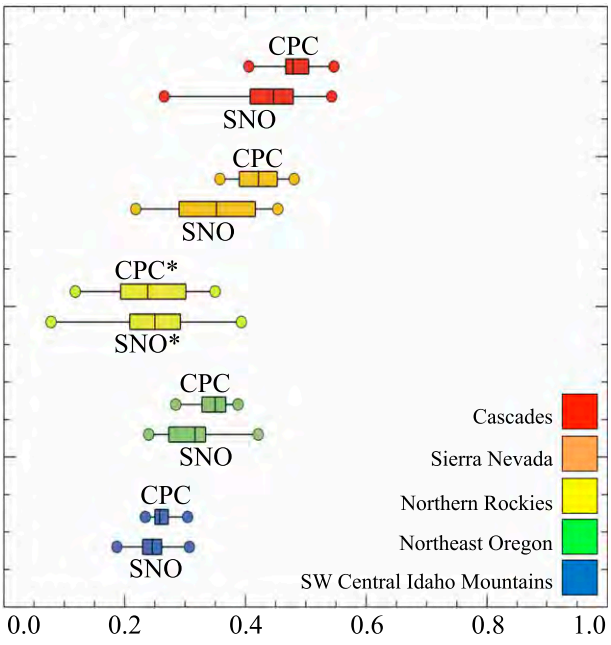

FIG. 9. Box and whisker diagram of IVT_{250} AR fraction for each region in Fig. 8b based on interpolation of CPC data to SNOTEL locations (CPC) and SNOTEL precipitation observations (SNO). Circles represent the (left) minimum and (right) maximum values. Vertical lines within each box and whisker plot represent the first quartile, median, and third quartile. Asterisks denote regions where the difference in median AR fraction between the CPC data and SNOTEL locations is not statistically significant at the 95% confidence level.

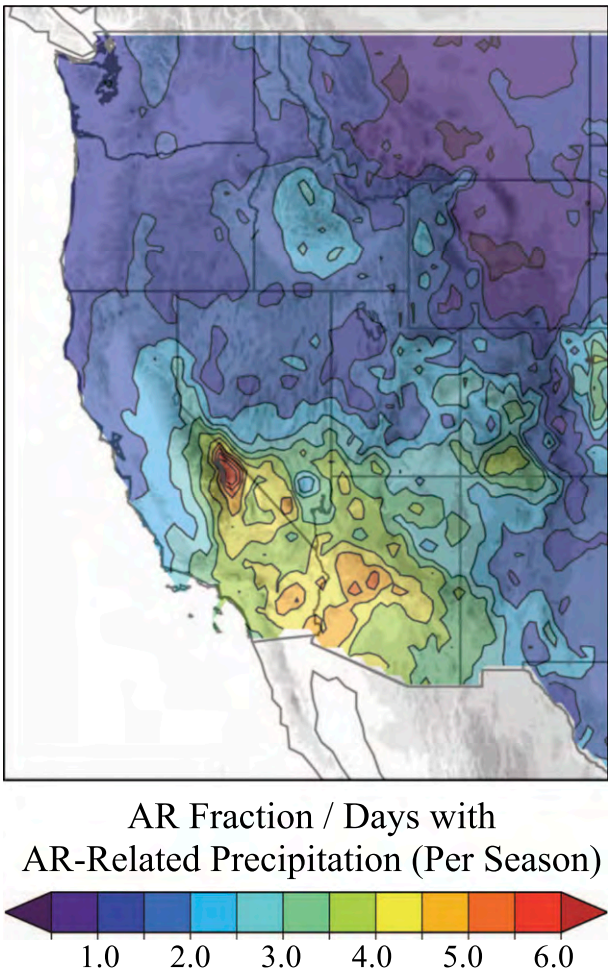

FIG. 10. Mean cool-season ratio of IVT_{250} AR fraction (multiplied by 100) to the number of days with AR-related precipitation.

a quasi-zonally oriented band that extends across the eastern Pacific, with a broad maxima near the Oregon and Northern California coast (Figs. 13e,f). At 0 h, the pattern is bifurcated with a primary (secondary) band of high values to the north (south) of the high Sierra. These bands merge into a maximum over northern Utah. This bifurcated pattern reflects two pathways for AR penetration into northern Utah, one to the north of the high Sierra, the other to the south. The 500-hPa composite features predominantly zonal flow, which does not reflect the dominant flow pattern, but rather an averaging of patterns associated with ARs penetrating into the Great Basin to the north or south of the high Sierra.

Similar results are obtained along nearby meridional transects, suggesting that two broad, favored pathways for AR penetration flank the high Sierra, with AR penetration into the interior northwest (southwest) typically occurring within regions of anticyclonic (cyclonic) curvature north (south) of this range. The intermediate eastern Great Basin represents a transition zone in which ARs are rare and short lived, but can be affected by AR pathways to the north or south of the high Sierra.

6. Discussion

In an Eulerian framework, the local time tendency of IVT is a function of IVT divergence, evaporation, and precipitation. Assuming no evaporation over land, IVT convergence increases IVT, while IVT divergence and precipitation decrease IVT. Hence, ARs defined on the basis of IVT are prone to rapid decay (i.e., the decrease in size and IVT magnitude, possibly to the point of disappearance of an AR) over the same regions where their effects (e.g., heavy precipitation and flooding) are most severe. Additionally, because of the climatological decrease of water vapor with height, IVT is typically sensitive to the surface pressure, which is much lower over

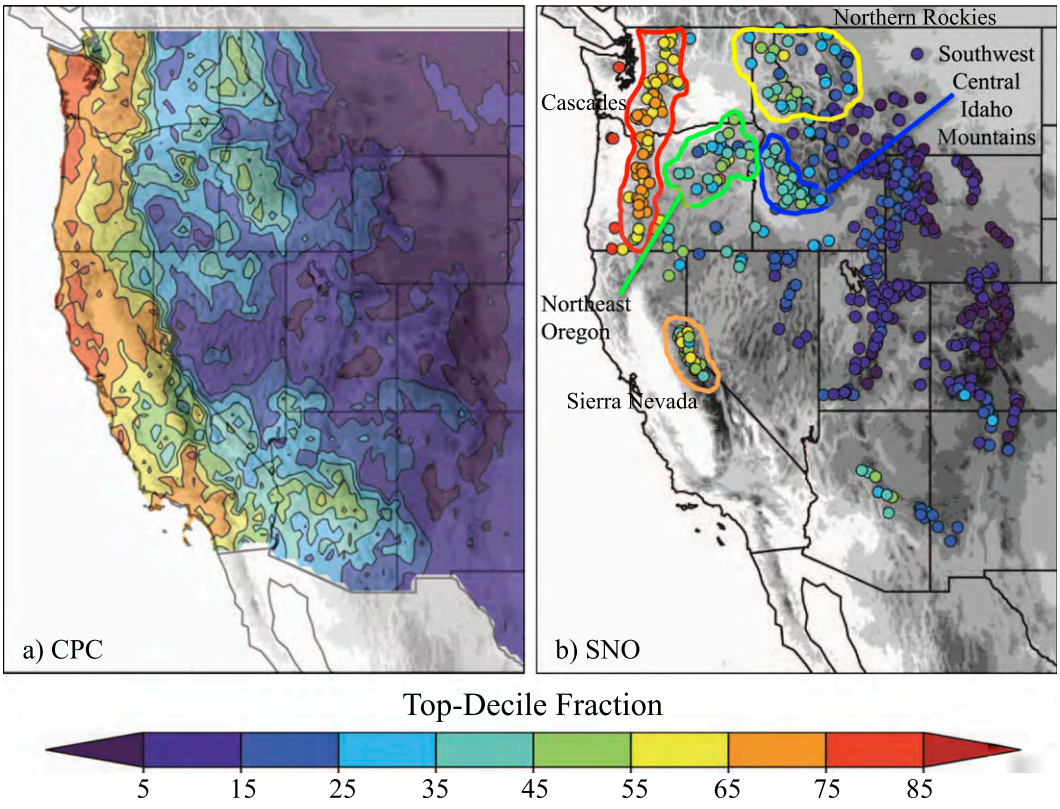

FIG. 11. As in Fig. 8, but for top-decile fraction (i.e., the fraction of top-decile 24-h precipitation events associated with ARs).

higher elevation regions, contributing to smaller IVT values.

With the above in mind, our results indicate that the climatology of ARs and AR-related precipitation over the western United States is strongly influenced by three major factors. The first is the climatological characteristics of ARs along the West Coast, which influences the frequency, intensity (i.e., the magnitude of IVT), duration, and orientation of ARs as they begin to penetrate into the interior. The second is the local depletion of water vapor by precipitation, especially as air moves over high mountain barriers, which contributes to AR decay by reducing the IWV and corresponding water vapor transport. The third is the general increase in surface elevation and decrease in pressure that occurs from the U.S. West Coast higher elevation locations in the interior.

Over the northwestern United States, the AR frequency decreases rapidly from the coast to the lee of the Cascades and then more gradually across the interior (Fig. 4a). An axis of high AR frequency and mean duration is found along a relatively low-elevation corridor that extends from the Columbia basin into northern Montana (Figs. 4 and 7). This leads to higher AR and top-decile fractions across northern Idaho and northwestern Montana, including Glacier National Park, than found over southwest Montana and the northeast central Idaho mountains (Fig. 8). A second axis of high AR frequency extends into the Snake River Plain and the adjoining central Idaho mountains. The strong, near-monotonic decrease in AR and top-decile fractions from southwest to northeast across the central Idaho mountains (Fig. 14) likely reflects vapor depletion and airmass transformation as orographic precipitation is generated in the westerly and southwesterly flow that frequently accompanies ARs over the region (e.g., Fig. 13). In contrast, the AR and top-decile fractions feature more spatial variability over northeast Oregon, northern Idaho, and northwestern Montana where the ranges lack a sustained high-mountain mass and feature a variety of orientations, geometries, and exposures to westerly and southwesterly flow.

Over the southwestern United States, the mountains of Southern California and the Baja Peninsula are narrower and less continuous than the Cascades–Sierra ranges, resulting in less airmass transformation and a more modest decline in AR frequency from the coast to the interior. Although the AR frequency is lower than

over the northwestern United States, the AR and top-decile fractions over southern and central Arizona are greater than those found east of the Oregon and Washington Cascades. This suggests that the occurrence or nonoccurrence of a small number of AR events strongly influences the cool-season hydroclimate of the southwest, a result that is broadly consistent with Dettinger et al. (2011).

Over the central Great Basin, ARs are short lived and rare, owing to the southward decrease in coastal AR frequency combined with the effects of the high Sierra. Additionally, the AR fraction and top-decile fraction are very low across this region. ARs that penetrate into the interior rarely extend over the high Sierra, which induce AR decay, but more frequently penetrate inland either to the north or south of this range (Fig. 13).

The AR fraction found in this study differs from that found by Dettinger et al. (2011) and Rutz and Steenburgh (2012). For example, this study finds a decrease in AR fraction from the West Coast to the lee of the Cascade–Sierra ranges, where a more abrupt decrease exists, particularly in the lee of the Sierra Nevada. In contrast, both Dettinger et al. (2011, see their Fig. 6) and Rutz and Steenburgh (2012, see their Fig. 3) show little decline in AR fraction from the coast to the lee of the Cascades [Rutz and Steenburgh (2012) even found higher AR fractions east of the Washington Cascades than to the west]. Dettinger et al. (2011) illustrate a decrease in AR fraction across the Sierra Nevada, but Rutz and Steenburgh (2012) find a maximum over the Sierra Nevada, with the strongest decrease farther to the east over central Nevada.

Fundamentally, these differences are likely produced by our geographically specific method of attributing precipitation to ARs, which accounts for the decay of inland-penetrating ARs, whereas Dettinger et al. (2011) and Rutz and Steenburgh (2012) simply attribute all western U.S. precipitation to ARs on the day of or day following AR observation along the coast, rather than at the inland gauge locations. Our method constrains precipitation attributed to ARs to that occurring only at locations where AR conditions are observed, resulting in a decline in inland AR-related precipitation due to AR decay. This approach offers the advantage of geographic specificity (e.g., non-AR precipitation in the northwest is not considered when there is an AR over the southwest), but also neglects precipitation that may be related to water vapor transport downstream from a decayed AR into the interior western United States. Ultimately, the definition of AR precipitation is somewhat ambiguous using daily totals [although Ralph et al. (2013a) found agreement between hourly resolved observations of AR conditions and precipitation at a key coastal observing site and findings by Dettinger et al. (2011) that used daily COOP precipitation observations in the region]. The method used here depends on daily data, applies a measure of geographic specificity, and accounts for AR penetration inland from the coast, thus providing a new perspective on the relationship between ARs and precipitation over the interior western United States.

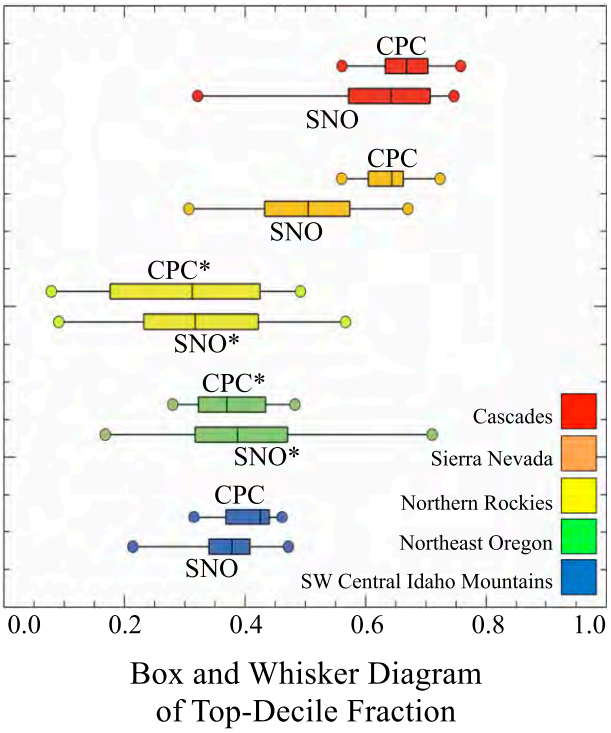

FIG. 12. As in Fig. 9, but for top-decile fraction.

Our findings also depend on the characteristics of the underlying datasets and the methodology used to identify ARs. First, the ERA-Interim model topography does not accurately represent the complex topography of the western United States (cf. Figs. 1a and 1b) and the full range of possible IVT values within each 1.5° × 1.5° grid box. We anticipate that a higher-resolution analysis would likely yield more filamentary AR structures (e.g., longer and narrower), possibly with greater inland penetration, but also with more spatial variability and greater fragmentation of the IVT_{250} region due to smaller-scale topographic effects. The current analysis provides a reasonable analysis of the regional characteristics of ARs over the western United States, but future work may be able to better quantify smaller-scale AR characteristics, such as those influenced by barrier jets that form on the upwind side of major mountains (e.g., Neiman et al. 2010; Hughes et al. 2012; Kingsmill et al. 2013).

Second, the AR characteristics are sensitive to the IVT threshold used. Although it appears that variations

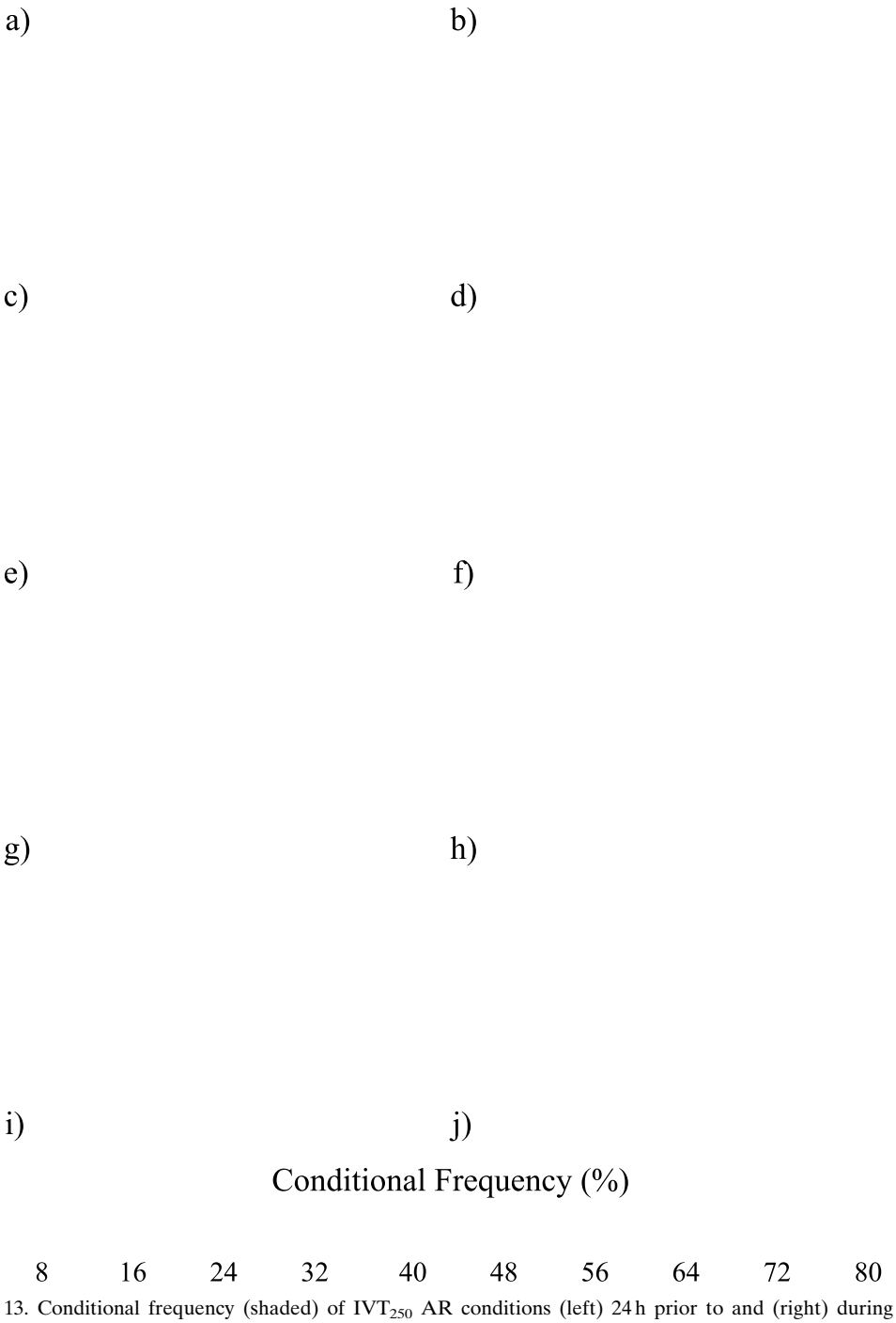

FIG. 13. Conditional frequency (shaded) of IVT_{250} AR conditions (left) 24 h prior to and (right) during the existence of AR conditions at selected locations (stars) along the 111°W meridian at (a),(b) 46.5°N; (c),(d) 43.5°N; (e),(f) 40.5°N; (g),(h) 37.5°N; and (i),(j) 34.5°N. Contours are the composite 500-hPa geopotential height.

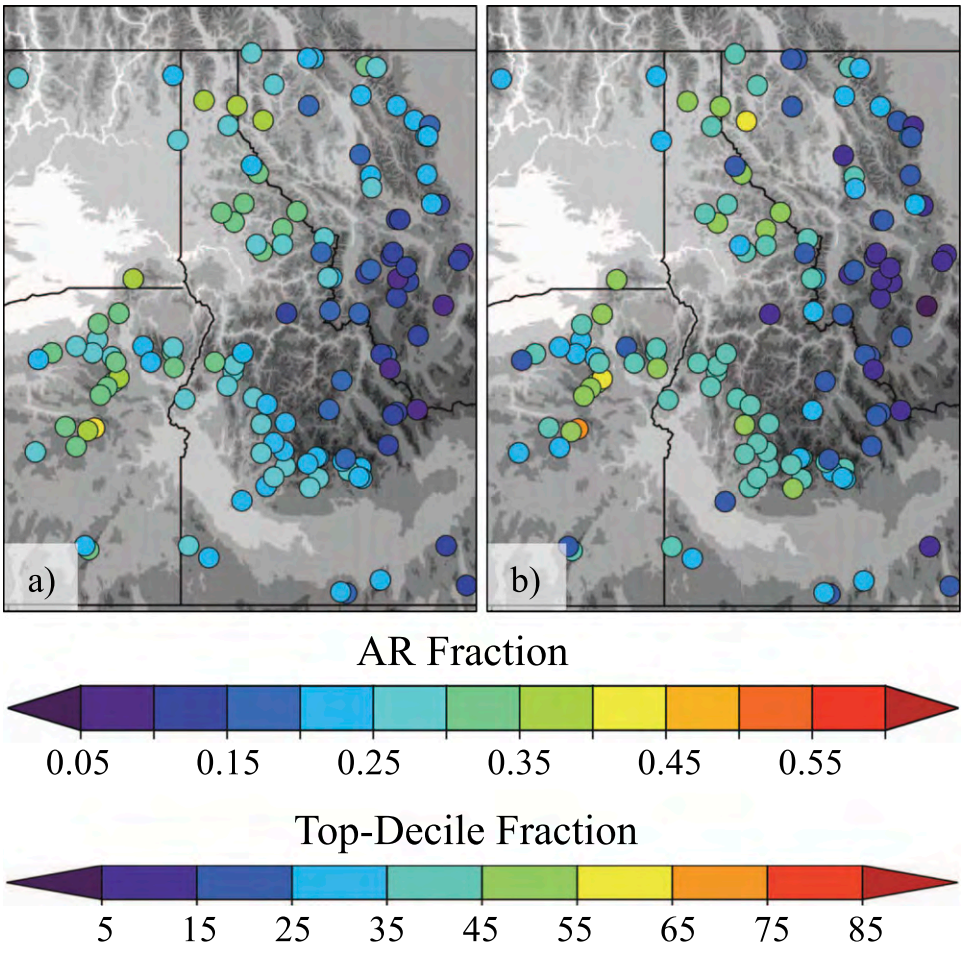

FIG. 14. (a) AR fraction and (b) top-decile fraction at SNOTEL stations over the interior northwestern United States.

in the IVT threshold do not strongly influence the spatial patterns of AR characteristics, they do affect the magnitude (e.g., Fig. 5). We also have not used a width criteria, as was done in previous studies (e.g., Ralph et al. 2004; Neiman et al. 2008b; Dettinger et al. 2011; Wick et al. 2013), although our inspection of individual events suggests this has little impact on the results.

Finally, one should consider the method we use to attribute precipitation totals to ARs, which requires that an AR be present at only one analysis time during the 24-h accumulation period. Increasing this threshold reduces the AR and top-decile fractions, but does not strongly affect the resulting geographic patterns (not shown).

7. Conclusions

This study has examined the climatological characteristics of cool-season (November–April) ARs and their influence on precipitation over the western United States. AR frequency is largest along the Oregon–Washington coast and decreases southward along the California coast. Over the interior, AR frequency is strongly influenced by the characteristics (e.g., frequency, intensity, duration, and orientation) of landfalling ARs along the West Coast and the subsequent loss of water vapor due to precipitation, especially over higher mountain barriers such as the high Sierra. Hence, AR frequency over the interior is largest over the northwest, particularly over low-elevation corridors that stretch into northwestern Montana and the Snake River Plain. In contrast, the smallest AR frequencies extend from just east of the high Sierra across the central Great Basin into the deep interior. The mean duration of AR conditions follows a spatial pattern similar to that of AR frequency, but is relatively high over the southwest interior.

AR-related cool-season precipitation, as represented by the AR fraction and top-decile fraction, is largest over the northwestern and southwestern United States.

Although ARs are relatively infrequent over the southwest, the fraction of cool-season precipitation and top-decile precipitation events they produce is comparable to that found over the northwest. Thus, the hydroclimate of the southwest is critically dependent on a small number of cool-season AR events. In contrast, the AR fraction and top-decile fraction are smallest over the Great Basin east of the high Sierra, which act to impede the inland penetration of ARs. The AR fraction and top-decile fraction feature substantial variability within some regions (e.g., northeast Oregon, northern Idaho, northwestern Montana), especially where the topography lacks a sustained high mountain mass and features complex orientations and geometries.

These results improve our understanding of the influence of ARs on the weather and climate of the western United States. Future work could examine the physical mechanisms that enable or prevent AR penetration into the interior, which could ultimately lead to a broad conceptual model that differentiates between penetrating and nonpenetrating ARs. An analysis of AR water budgets, particularly as ARs interact with major topographical barriers, could provide additional insight for this model. The results of this work would have a broad range of implications, from short-term forecasting to water management issues in a changing climate.

Acknowledgments. We thank Trevor Alcott, Jason Cordeira, Darren Jackson, Gary Wick, and one anonymous reviewer for comments and suggestions that improved the manuscript. We also thank Andy Edman, John Horel, Mimi Hughes, Kelly Mahoney, Ben Moore, Paul Neiman, Court Strong, and Ellen Sukovich for discussions that facilitated additional improvement. We gratefully acknowledge the provision of datasets, software, and or computer time and services provided by ECMWF, NOAA/NWS CPC, USDA/NRCS, and the University of Utah Center for High Performance Computing. This article is based on research supported by a series of grants from the NOAA/National Weather Service CSTAR Program. Any opinions, findings, and conclusions or recommendations expressed herein are those of the authors and do not necessarily reflect those of the NOAA/National Weather Service.

REFERENCES

Bao, J.-W., S. A. Michelson, P. J. Neiman, F. M. Ralph, and J. M. Wilczak, 2006: Interpretation of enhanced integrated water vapor bands associated with extratropical cyclones: Their formation and connection to tropical moisture. *Mon. Wea. Rev.,* **134,** 1063–1080.

Bernhardt, D., 2006: Glacier National Park flooding November 2006. NWS Western Region Tech. Attachment 08-23, 15 pp.

Berrisford, P., D. Dee, K. Fielding, M. Fuentes, P. Kallberg, S. Kobayashi, and S. Uppala, 2009: The ERA-Interim archive. ECMWF Tech. Rep. 1, 16 pp. [Available online at http://www.ecmwf.int/publications/library/do/references/show?id=89203.]

Browning, K. A., 1971: Radar measurements of air motion near fronts. *Weather,* **26,** 320–340.

Carlson, T. N., 1980: Airflow through midlatitude cyclones and the comma cloud pattern. *Mon. Wea. Rev.,* **108,** 1498–1509.

Dee, D. P., and Coauthors, 2011: The ERA-Interim reanalysis: Configuration and performance of the data assimilation system. *Quart. J. Roy. Meteor. Soc.,* **137,** 553–597, doi:10.1002/qj.828.

Dettinger, M. D., F. M. Ralph, T. Das, P. J. Neiman, and D. R. Cayan, 2011: Atmospheric rivers, floods, and the water resources of California. *Water,* **2011** (3), 445–478, doi:10.3390/w3020445.

Eckhardt, S., A. Stohl, H. Wernli, P. James, C. Forster, and N. Spichtinger, 2004: A 15-year climatology of warm conveyor belts. *J. Climate,* **17,** 218–237.

Guan, B., N. P. Molotch, D. E. Waliser, E. J. Fetzer, and P. J. Neiman, 2010: Extreme snowfall events linked to atmospheric rivers and surface air temperature via satellite measurements. *Geophys. Res. Lett.,* **37,** L20401, doi:10.1029/2010GL044696.

Hart, K. A., W. J. Steenburgh, and D. J. Onton, 2005: Model forecast improvements with decreased horizontal grid spacing over finescale intermountain orography during the 2002 Olympic Winter Games. *Wea. Forecasting,* **20,** 558–576.

Higgins, R. W., W. Shi, E. Yarosh, and R. Joyce, 2000: *Improved United States Precipitation Quality Control System and Analysis.* NCEP/Climate Prediction Center Atlas 7, NCEP/CPC. [Available online at http://www.cpc.ncep.noaa.gov/products/outreach/research_papers/ncep_cpc_atlas/7/.]

Hughes, M., P. J. Neiman, E. Sukovich, and F. M. Ralph, 2012: Representation of the Sierra Barrier Jet in 11 years of a high-resolution dynamical reanalysis downscaling compared with long-term wind profiler observations. *J. Geophys. Res.,* **117,** D18116, doi:10.1029/2012JD017869.

Junker, N. W., R. H. Grumm, R. Hart, L. F. Bosart, K. M. Bell, and F. J. Pereira, 2008: Use of normalized anomaly fields to anticipate extreme rainfall in the mountains of northern California. *Wea. Forecasting,* **23,** 336–356.

Kanamitsu, M., 1989: Description of the NMC Global Data Assimilation and Forecast System. *Wea. Forecasting,* **4,** 335–342.

Kingsmill, D. K., P. J. Neiman, B. J. Moore, M. Hughes, S. E. Yuter, and F. M. Ralph, 2013: Kinematic and thermodynamic structures of Sierra barrier jets and overrunning atmospheric rivers during a landfalling winter storm in Northern California. *Mon. Wea. Rev.,* **141,** 2015–2036.

Lavers, D. A., R. P. Allen, E. F. Wood, G. Villarini, D. J. Brayshaw, and A. J. Wade, 2011: Winter floods in Britain are connected to atmospheric rivers. *Geophys. Res. Lett.,* **38,** L23803, doi:10.1029/2011GL049783.

Moore, B. J., P. J. Neiman, F. M. Ralph, and F. E. Barthold, 2012: Physical processes associated with heavy flooding rainfall in Nashville, Tennessee, and vicinity during 1–2 May 2010: The role of an atmospheric river and mesoscale convective systems. *Mon. Wea. Rev.,* **140,** 358–378.

Neiman, P. J., F. M. Ralph, A. B. White, D. E. Kingsmill, and P. O. G. Persson, 2002: The statistical relationship between upslope flow and rainfall in California's Coastal Mountains:

Observations during CALJET. *Mon. Wea. Rev.,* **130,** 1468–1492.

——, ——, G. A. Wick, Y.-H. Kuo, T.-K. Wee, Z. Ma, G. H. Taylor, and M. D. Dettinger, 2008a: Diagnosis of an intense atmospheric river impacting the Pacific Northwest: Storm summary and offshore vertical structure observed with COSMIC satellite retrievals. *Mon. Wea. Rev.,* **136,** 4398–4420.

——, ——, ——, J. D. Lundquist, and M. D. Dettinger, 2008b: Meteorological characteristics and overland precipitation impacts of atmospheric rivers affecting the west coast of North America based on eight years of SSM/I satellite observations. *J. Hydrometeor.,* **9,** 22–47.

——, E. M. Sukovich, F. M. Ralph, and M. Hughes, 2010: A seven-year wind profiler-based climatology of the windward barrier jet along California's Sierra Nevada. *Mon. Wea. Rev.,* **138,** 1206–1233.

——, L. J. Schick, F. M. Ralph, M. Hughes, and G. A. Wick, 2011: Flooding in western Washington: The connection to atmospheric rivers. *J. Hydrometeor.,* **12,** 1337–1358.

——, F. M. Ralph, B. J. Moore, M. Hughes, K. M. Mahoney, J. M. Cordeira, and M. D. Dettinger, 2013: The landfall and inland penetration of a flood-producing atmospheric river in Arizona. Part I: Observed synoptic-scale, orographic, and hydrometeorological characteristics. *J. Hydrometeor.,* **14,** 460–464.

Newell, R. E., and Y. Zhu, 1994: Tropospheric rivers: A one-year record and a possible application to ice core data. *Geophys. Res. Lett.,* **21,** 113–116.

——, N. E. Newell, Y. Zhu, and C. Scott, 1992: Tropospheric rivers?—A pilot study. *Geophys. Res. Lett.,* **19,** 2401–2404.

Ralph, F. M., P. J. Neiman, and G. A. Wick, 2004: Satellite and CALJET aircraft observations of atmospheric rivers over the eastern North Pacific Ocean during the winter of 1997/98. *Mon. Wea. Rev.,* **132,** 1721–1745.

——, ——, ——, S. I. Gutman, M. D. Dettinger, D. R. Cayan, and A. B. White, 2006: Flooding on California's Russian River: Role of atmospheric rivers. *Geophys. Res. Lett.,* **33,** L13801, doi:10.1029/2006GL026689.

——, ——, G. N. Kiladis, K. Weickmann, and D. W. Reynolds, 2011: A multiscale observational case study of a Pacific atmospheric river exhibiting tropical–extratropical connections and a mesoscale frontal wave. *Mon. Wea. Rev.,* **139,** 1169–1189.

——, T. Coleman, P. J. Neiman, R. J. Zamora, and M. D. Dettinger, 2013a: Observed impacts of duration and seasonality of atmospheric-river landfalls on soil moisture and runoff in coastal northern California. *J. Hydrometeor.,* **14,** 443–459.

——, and Coauthors, 2013b: The emergence of weather-related test beds linking research and forecasting operations. *Bull. Amer. Meteor. Soc.,* **94,** 1187–1211.

Rasmussen, R., and Coauthors, 2011: High-resolution coupled climate runoff simulations of seasonal snowfall over Colorado: A process study of current and warmer climate. *J. Climate,* **24,** 3015–3048.

Rigby, J. G., 1998: The 1997 New Year's floods in western Nevada. Special Publication 23, Nevada Bureau of Mines and Geology, University of Nevada, Reno, NV, 111 pp.

Rutz, J. J., and W. J. Steenburgh, 2012: Quantifying the role of atmospheric rivers in the interior western United States. *Atmos. Sci. Lett.,* **13,** 257–261, doi:10.1002/asl.392.

Serreze, M. C., M. P. Clark, R. L. Armstrong, D. A. McGinnis, and R. S. Pulwarty, 1999: Characteristics of the western United States snowpack telemetry (SNOTEL) data. *Water Resour. Res.,* **35** (7), 2145–2160.

Simmons, A., S. Uppala, D. Dee, and S. Kobayashi, 2007: ERA-Interim: New ECMWF reanalysis products from 1989 onwards. *ECMWF Newsletter,* No. 110, ECMWF, Reading, United Kingdom, 25–35.

Smith, B. L., S. E. Yuter, P. J. Neiman, and D. E. Kingsmill, 2010: Water vapor fluxes and orographic precipitation over northern California associated with a landfalling atmospheric river. *Mon. Wea. Rev.,* **138,** 74–100.

Smith, R. B., I. Barstad, and L. Bonneau, 2005: Orographic precipitation and Oregon's climate transition. *J. Atmos. Sci.,* **62,** 177–191.

Sodemann, H., and A. Stohl, 2013: Moisture origin and meridional transport in atmospheric rivers and their association with multiple cyclones. *Mon. Wea. Rev.,* **141,** 2850–2868.

Stohl, A., C. Forster, and H. Sodemann, 2008: Remote sources of water vapor forming precipitation on the Norwegian west coast at 60°N—A tale of hurricanes and an atmospheric river. *J. Geophys. Res.,* **113,** D05102, doi:10.1029/2007JD009006.

Uppala, S., D. Dee, S. Kobayashi, P. Berrisford, and A. Simmons, 2008: Towards a climate data assimilation system: Status update of ERA-Interim. *ECMWF Newsletter,* No. 115, ECMWF, Reading, United Kingdom, 12–18. [Available online at http://www.ecmwf.int/publications/newsletters/pdf/115.pdf.]

USDA-NRCS, 2012a: SNOTEL and snow survey & water supply forecasting. USDA-NRCS, 2 pp. [Available online at http://www.wcc.nrcs.usda.gov/snotel/SNOTEL-brochure.pdf.]

——, cited 2012b: SNOTEL data collection network fact sheet. [Available online at http://www.wcc.nrcs.usda.gov/factpub/sntlfct1.html.]

U.S. Department of the Interior, 2012: Flood of January 1997 in the Truckee River Basin, Western Nevada. USGS, 2 pp. [Available online at http://pubs.usgs.gov/fs/1997/0123/report.pdf.]

Viale, M., and M. N. Nuñez, 2011: Climatology of winter orographic precipitation over the subtropical central Andes and associated synoptic and regional characteristics. *J. Hydrometeor.,* **12,** 481–507.

Warner, M. D., C. F. Mass, and E. P. Salathé, 2012: Wintertime extreme precipitation events along the Pacific Northwest coast: Climatology and synoptic evolution. *Mon. Wea. Rev.,* **140,** 2021–2043.

Wick, G. A., P. J. Neiman, and F. M. Ralph, 2013: Description and validation of an automated objective technique for identification and characterization of the integrated water vapor signature of atmospheric rivers. *IEEE Trans. Geosci. Remote Sens.,* **51** (4), 2166–2176, doi:10.1109/TGRS.2012.2211024.

Zhu, Y., and R. E. Newell, 1998: A proposed algorithm for moisture fluxes from atmospheric rivers. *Mon. Wea. Rev.,* **126,** 725–735.